Radiation Measurements 82 (2015) 93–101

Contents lists available at ScienceDirect

Radiation Measurements

journal homepage: www.elsevier.com/locate/radmeas

On the effect of optical and isothermal treatments on luminescence signals from feldspars

Vasilis Pagonis [a, *], George Polymeris [b], George Kitis [c]

[a] Physics Department, McDaniel College, Westminster, MD 21157, USA
[b] Institute of Nuclear Sciences, Ankara University, 06100 Besevler, Ankara, Turkey
[c] Nuclear Physics Laboratory, Aristotle University of Thessaloniki, 54124 Thessaloniki, Greece

HIGHLIGHTS

- CW-IRSL and CW-OSL measurements are preceded by heating or optical bleaching.
- New analytical equations are derived to describe these double experimental procedures.
- Equations are compared with data from a feldspar sample following isothermal procedure.
- Equations are compared with data from a feldspar sample following optical bleaching.

ARTICLE INFO

Article history:
Received 13 March 2015
Received in revised form
23 July 2015
Accepted 7 September 2015
Available online 9 September 2015

Keywords:
Infrared stimulated luminescence emission
Apatites
Tunneling
Kinetic model

ABSTRACT

During luminescence dosimetry and luminescence dating applications it is often necessary to precondition the geological samples by applying a thermal or optical treatment before measuring the luminescence signal. In luminescence applications using apatites or feldspars, measurement of continuous-wave infrared or optically stimulated signals (CW-IRSL and CW-OSL) are customarily preceded by either an isothermal heating of the samples at a fixed temperature for a short time interval, or alternatively by optically bleaching the samples using light from LEDs with the appropriate wavelength. This paper presents new analytical equations which can be used to describe these commonly employed double experimental procedures. The equations are based on a recently published model which assumes that tunneling processes are taking place in random distributions of donor–acceptor pairs. The concentration of charge carriers during the CW-IRSL or CW-OSL experiment is expressed in terms of the parameters of the preceding thermal or optical bleaching procedure, and depends also on the distribution of distances between electron and hole pairs. The analytical equations in this paper are compared with experimental data from a feldspar sample which undergoes an isothermal procedure followed by measurement of the CW-IRSL signal. Additional comparisons with experiment are provided using a feldspar sample which undergoes an infrared bleaching process, followed by measurement of the CW-OSL signal. These results and conditions under which the equations can be used are discussed within the framework of the model.

1. Introduction

During the past decade there has been significant progress in our understanding of luminescence processes in feldspars. In particular recent experimental and modeling work has helped researchers understand the non-exponential shape of continuous-wave infrared stimulated luminescence (CW-IRSL) signals from feldspars (Li and Li, 2013; Morthekai et al., 2012; Jain and Ankjærgaard, 2011; Thomsen et al., 2011; Bailiff and Poolton, 1991).

Specifically the model developed by Jain et al. (2012) has been a major development in this research area, and has helped in the understanding of tunneling phenomena in a random distribution of electron–hole pairs. Kitis and Pagonis (2013) quantified the semi-analytical model of Jain et al. (2012) by deriving exact analytical expressions for different experimental stimulation modes. This was used to describe luminescence signals from a variety of feldspars

* Corresponding author.
E-mail address: vpagonis@mcdaniel.edu (V. Pagonis).

http://dx.doi.org/10.1016/j.radmeas.2015.09.002
1350-4487/

and apatites (Polymeris et al., 2014; Sfampa et al., 2014; Pagonis et al., 2013). In a recent comprehensive study Pagonis et al. (2014a) examined CW-IRSL signals from a variety of feldspars and described mathematically the shape of these signals in terms of the kinetic parameters in the model of Jain et al. (2012). Kitis and Pagonis (2014) simulated the geometrical shape factor of thermoluminescence (TL) glow curves within the model, and showed that standard kinetic methods of initial rise and variable heating rate can be used to obtain the kinetic parameters for the TL process. Pagonis et al. (2013) obtained approximate expressions for the time development of nearest neighbor distribution during various types of luminescence experiments, and compared their analytical expressions with experimental data on linearly modulated IRSL (Bulur, 1996).

During luminescence dosimetry and luminescence dating applications it is often necessary to precondition the geological samples by applying a thermal or optical treatment before measuring the luminescence signal. In luminescence applications using apatites or feldspars, measurements of CW-IRSL or optically stimulated signals (CW-OSL) are customarily preceded by either an isothermal heating of the samples at a fixed temperature for a short time interval, or alternatively by optically bleaching the samples using light from LEDs with the appropriate wavelength. Murray et al. (2009) reviewed previous research on the effect of preheating on the IRSL signal from feldspar (Bøtter-Jensen et al., 2003; Duller and Bøtter-Jensen, 1993; Duller, 1994; Duller and Wintle, 1991). These authors concluded that IR stimulation is changing the luminescence recombination probability. They proposed that electrons are not necessarily stimulated from the TL traps by IR, but the loss of recombination sites during measurement of the IRSL signal causes a reduction of the photon yield during subsequent measurement of the luminescence signal. Recently Pagonis et al. (2014b) reviewed previous research on the shape and kinetics of TL glow curves in feldspars, on possible correlations between TL and IRSL signals and on the effect of IR illumination on the TL signal (Duller, 1995; Visocekas et al., 1994; Chruścińska, 2001).

In an important recent work Jain et al. (2015) extended their localized transition model to include Arrhenius analysis and for truncated nearest neighbor distributions. Their extended model successfully described the thermal and optical kinetic behavior of IRSL signals from preheated feldspar samples, and was tested using experimental data. These authors found that different infrared stimulated luminescence emissions (UV, blue, yellow and far-red) follow the same kinetics, and most likely involve the same electron trap. A key result of their analysis is that a prior-treatment results in a shifted time domain of the luminescence data.

Pagonis et al. (2013) examined the exact version of the model developed by Jain et al. (2012), and developed analytical equations for the concentration of carriers during measurement of luminescence signals, as a function of two parameters, namely the distance between electron–hole pairs and the stimulation time.

This paper uses the analytical equations developed by Pagonis et al. (2013), in an attempt to describe double experimental procedures commonly used during luminescence dating and luminescence dosimetry protocols.

The goals of the present paper are:

(a) To develop an alternative mathematical approach to the work by Jain et al. (2015), by starting from the analytical equations derived by Pagonis et al. (2013).
(b) The specific goal of this new approach is to develop analytical equations for the intensity of continuous-wave stimulated luminescence (CW-IRSL or CW-OSL) signals for samples which have been pre-treated either optically or thermally. The equations developed in this paper are shown to be a special case of the more general formalism of Jain et al. (2015).
(c) To test the analytical equations by comparing with experimental data from a feldspar sample which undergoes an isothermal procedure, followed by measurement of the CW-IRSL signal. Similarly, the equations are tested for a sample which is first bleached using IR, followed by measurement of the CW-OSL signal.
(d) To discuss the experimental results within the framework of the model, and to also consider the conditions under which the analytical equations can be used to analyze experimental data.

2. Analytical equations for double experimental procedures

In this section analytical equations are developed for the time dependent concentration of charge carriers during two commonly used experimental procedures. In Section 2.1 we consider a freshly irradiated sample which undergoes an isothermal procedure (heating at a fixed temperature for a certain amount of time), followed by measurement of the CW-IRSL signal. In Section 2.2 a freshly irradiated sample undergoes an optical bleaching, followed again by measurement of the CW-IRSL or CW-OSL signal.

2.1. Isothermal procedure followed by measurement OF CW-IRSL signal

Kitis and Pagonis (2013) showed that the concentration of charge carriers during optical or thermal stimulation in the model by Jain et al. (2012) is given by

$$n(r',t) = n_0 3(r')^2 \exp\left[-(r')^3\right] \exp\left[-\exp\left(-(\rho')^{-1/3} r'\right) \int_0^t A dt'\right], \tag{1}$$

where A represents the probability of thermal/optical stimulation and ρ' is the dimensionless charge density. Equation (1) describes the evolution of the distribution of electrons $n(r',t)$ in the ground state as a function of two parameters, namely the time t elapsed since the beginning of the optical or thermal stimulation, and the dimensionless distance parameter r'. This equation is valid for several types of excitation used in typical TL or OSL experiments, and the integral $\int_0^t A dt'$ can be evaluated for the different experimental excitation modes. During an isothermal preheat experiment the probability of thermal excitation $A = A_{PH}$ = constant, and Equation (1) becomes:

$$n(r',t) = n_0 3(r')^2 \exp\left[-(r')^3\right] \exp\left[-\exp\left(-(\rho')^{-1/3} r'\right) A_{PH} t\right], \tag{2}$$

where n_o is the total initial concentration of charge carriers, and the quantity A_{PH} (s^{-1}) represents the probability of thermal stimulation given by:

$$A_{PH} = s_{thermal} e^{-E_{thermal}/kT_{PH}}, \tag{3}$$

where T_{PH} is the preheat temperature and $s_{thermal}$, $E_{thermal}$ represent the thermal kinetic parameters of the trap. At the end of the preheat process at a temperature T_{PH} and for a time interval t_{PH}, the distribution of remaining electron–hole pairs are then:

$$n(r',t_{PH}) = n_0 3(r')^2 \exp\Big[-(r')^3\Big]\exp\Big[-\exp\Big(-(\rho')^{-1/3}r'\Big)s_{thermal}e^{-E_{thermal}/kT_{PH}}t_{PH}\Big]. \quad (4)$$

The key point in this section is that this distribution of carriers $n(r',t_{PH})$ will act as the initial concentration of carriers for the second stage of the double procedure during which one measures the CW-IRSL signal.

During a CW-IRSL measurement the probability of optical (IR) excitation is $A = A_{IR}$ = constant, and Equation (1) becomes:

$$n_{IR}(r',t) = N_0(r')\exp\Big[-\exp\Big(-(\rho')^{-1/3}r'\Big)A_{IR}t\Big]. \quad (5)$$

where $N_0(r') = n(r',t_{PH})$ is the initial distribution of charge carriers at the beginning of the CW-IRSL measurement, and the quantity A_{IR} (s^{-1}) represents the probability of infrared stimulation. The value of$A_{IR} = \sigma I$ depends on the infrared photostimulation cross section $\sigma(cm^2)$ and on the intensity I (photons. cm^{-2}. s^{-1}) of the optical source.

By substituting (4) into (5), one obtains:

$$\begin{aligned} n_{IR}(r',t) &= n_0 3(r')^2 \exp\Big[-(r')^3\Big]\exp\Big[-\exp\Big(-(\rho')^{-1/3}r'\Big)s_{thermal}e^{-E_{thermal}/kT_{PH}}t_{PH}\Big].\exp\Big[-\exp\Big(-(\rho')^{-1/3}r'\Big)A_{IR}t\Big] \\ &= n_0 3(r')^2 \exp\Big[-(r')^3\Big]\exp\Big[-\exp\Big(-(\rho')^{-1/3}r'\Big)\Big\{s_{thermal}e^{-E_{thermal}/kT_{PH}}t_{PH} + A_{IR}t\Big\}\Big] \end{aligned} \quad (6)$$

or

$$n_{IR}(r',t) = n_0 3(r')^2 \exp\Big[-(r')^3\Big]\exp\Big[-\exp\Big(-(\rho')^{-1/3}r'\Big)A_{IR}\Big\{\frac{s_{thermal}}{A_{IR}}e^{-E_{thermal}/kT_{PH}}t_{PH} + t\Big\}\Big] \quad (7)$$

This equation can be written as:

$$n_{IR}(r',t) = n_0 3(r')^2 \exp\Big[-(r')^3\Big]\exp\Big[-\exp\Big(-(\rho')^{-1/3}r'\Big)A_{IR}\{T+t\}\Big], \quad (8)$$

where we have defined the constant time parameter

$$T = \frac{s_{thermal}}{A_{IR}}e^{-E_{thermal}/kT_{PH}}t_{PH}. \quad (9)$$

Equation (9) is a new result derived in this paper for preheated samples, and similarly Equation (21) is the corresponding new equation derived for optically bleached samples.

For an untreated sample, one sets $t_{PH} = 0$ in Equation (8), to obtain the corresponding concentration of charge carriers during the CW-IRSL measurement:

$$n_{IR-UNTREATED}(r',t) = n_0 3(r')^2 \exp\Big[-(r')^3\Big]\exp\Big[-\exp\Big(-(\rho')^{-1/3}r'\Big)\{A_{IR}t\}\Big]. \quad (10)$$

Direct comparison of Equations (8) And (10) shows that the two distributions $n_{IR}(r',t)$ and $n_{IR-UNTREATED}(r',t)$, for the preheated sample and for the untreated sample correspondingly, have the exact same mathematical form, with the time variable shifted by the constant factor T given in Equation (9). This shifting T of the time variable depends linearly on the preheat time t_{PH}, and depends also on the preheat temperature T_{PH} via the Boltzmann factor $e^{-E_{thermal}/kT_{PH}}$.

By integrating Equation (8) over the distance variable r', one finds the remaining number of electrons in the ground state at time t during the CW-IRSL experiment:

$$n_{IR}(t) = \int_0^\infty n_0 3(r')^2 \exp\Big[-(r')^3\Big]\exp\Big[-\exp\Big(-(\rho')^{-1/3}r'\Big)A_{IR}\{T+t\}\Big]dr', \quad (11)$$

or by using the shifted time variable $t' = T + t$:

$$n_{IR}(t) = \int_0^\infty n_0 3(r')^2 \exp\Big[-(r')^3\Big]\exp\Big[-\exp\Big(-(\rho')^{-1/3}r'\Big)A_{IR}t'\Big]dr' \quad (12)$$

This is the well-known equation that appears for example in Huntley (2006, Equation (4)) in the form:

$$\begin{aligned} n_{IR}(t) &= \int_0^\infty n_0 3(r')^2 \exp\Big[-(r')^3\Big]\exp\Big[-\exp\Big(-\frac{t}{\tau}\Big)\Big]dr' \\ &= \int_0^\infty n_0 3(r')^2 \exp\Big[-(r')^3\Big]\exp\Big[-\exp\Big(-(\rho')^{-1/3}r'\Big)st\Big]dr' \end{aligned} \quad (13)$$

In a recent work Pagonis et al. (2015, accepted) showed that based on a series expansion introduced by Tachiya and Mozumder (1974), the numerical integration in Equation (13) can be approximated to a great degree of accuracy by the expression:

$$n(t) = n_o \exp\Big[-\rho'\{\ln(zst)\}^3\Big]. \quad (14)$$

where $z = 1.8$ represents a numerical constant whose value was explained mathematically by Pagonis et al. (2015, accepted, the Appendix A). From a physical point of view, Jain et al. (2012, 2015) provided a physical meaning for this factor z, as representing the time derivative of the critical lifetime τ_c in the semi-analytical version of their model, i.e. $z \approx d\tau_c/dt$.

Comparison of Equations (12) and (13) shows that the solution of (12) can be obtained from the solution of Equation (13) by replacing s withA_{IR}, and t with t'. Therefore by making these substitutions in Equation (14), the solution of Equation (12) is given to a good approximation by:

$$n_{IR}(t) = n_o \exp\Big[-\rho'\{\ln(zA_{IR}t')\}^3\Big]. \quad (15)$$

The corresponding expression for the untreated sample is found by setting $t_{PH} = 0$ or $t' = t$, to obtain:

$$n_{IR-UNTREATED}(t) = n_o \exp\left[-\rho'\{\ln(zA_{IR}t)\}^3\right]. \quad (16)$$

The luminescence intensities for the thermally treated and the untreated sample correspondingly are found from the time derivatives of Equations (15) and (16):

$$L(t) = -\frac{dn_{IR}(t)}{dt} = C\frac{\exp\left[-\rho'\{\ln(zA_{IR}t')\}^3\right]\{\ln(zA_{IR}t')\}^2}{t'} \quad (17)$$

$$L_{UNTREATED}(t) = -\frac{dn_{IR-UNTREATED}(t)}{dt} = D\frac{\exp\left[-\rho'\{\ln(zA_{IR}t)\}^3\right]\{\ln(zA_{IR}t)\}^2}{t}, \quad (18)$$

with C, D representing constants.

Equations (17) and (18) lead to the obvious conclusion that the CW-IRSL luminescence intensities for the thermally treated and the untreated samples are described with the same equation, with the time-axis shifted by the quantity T given in Equation (9). This is the same result obtained previously by Jain et al. (2015) by considering the semi-analytical version of their original model. Specifically Equation (17) is a special case of the more general equation derived by Jain et al. (2015), by considering truncated distributions of nearest neighbors.

The kinetic parameters in Equation (17) are ρ', A_{IR} and can be obtained by fitting the time-shifted experimental data.

Furthermore, when the luminescence decay curve $L(t)$ for the thermally treated sample with different preheating times are shifted along the time-axis by the quantity T, the CW-IRSL decay curves can be expected to fall on top of each other, at least within the experimental uncertainties of the data. This is again the same result previously derived by Jain et al. (2015).

It is also noteworthy that Equation (18) for thermally *untreated* samples is almost identical to the following analytical equation derived by Kitis and Pagonis (2013) by examination of the semi-analytical version of the model by Jain et al. (2012):

$$L(t) = B\frac{\exp\left[-\rho'\{\ln(1+zA_{IR}t)\}^3\right][\ln(1+zAt)]^2}{1+zAt}. \quad (19)$$

The extra (1+) factor appearing in Equation (19) is often several orders of magnitude smaller numerically than the term zAt, so for all practical purposes Equations (18) and (19) give the exact same numerical results, for thermally untreated samples.

2.2. Optical bleaching procedure followed by measurement of the luminescence signal

In this section we consider a second type of experiment, in which the freshly irradiated sample is optically bleached in the first part of the experiment by exposure to either infrared light, or to blue light from LEDs (~470 nm). The analytical expressions are derived in this section for the case of an irradiated sample which is bleached optically by exposure to blue light for a time interval t_{BLEACH} (CW-OSL), followed by measurement of its CW-IRSL signal. However, the exact same equations can be derived for the reverse type of double procedure, in which the irradiated sample is first exposed to IR (CW-IRSL) for a time interval t_{BLEACH}, followed by measurement of its CW-OSL signal.

The main assumption in deriving the equations in this section is that the blue light (CW-OSL) accesses the same charge density ρ' as the IR light (IRSL), but with a different optical stimulation probability. This is a reasonable yet arbitrary physical assumption, which needs to be verified by the experimental data.

During the optical bleaching part of the double experiment, the probability of optical (blue light) excitation $A = A_{BLEACH} =$ constant, and the optical bleaching process takes place for a time interval t_{BLEACH}. We can now follow the same procedure as in Section 2.1, by assuming that the distribution of remaining electron–hole pairs at the end of the bleaching interval t_{BLEACH} will act as the initial concentration of carriers for the second stage of the double procedure, during which one measures the CW-IRSL signal. The probability of optical (IR) excitation during the CW-IRSL measurement is denoted once more by $A = A_{IR} =$ constant. By following the same steps as in Section 2.1, we obtain:

$$n_{IR}(r', t) = n_0 3(r')^2 \exp\left[-(r')^3\right]\exp\left[-\exp\left(-(\rho')^{-1/3}r'\right)A_{IR}\{T_{OPTICAL} + t\}\right], \quad (20)$$

where we have defined the constant time parameter

$$T_{OPTICAL} = \frac{A_{BLEACH}t_{BLEACH}}{A_{IR}}. \quad (21)$$

Equation (21) is the second new result derived in this paper for bleached samples, similar to Equation (9) derived for preheated samples.

This shifting $T_{OPTICAL}$ of the time variable depends linearly on the optical bleaching time t_{BLEACH}, and is also proportional to the ratio of excitation probabilities $\frac{A_{BLEACH}}{A_{IR}}$.

Equations (20) and (21) are completely analogous to (8) and (9), and lead to the same equations for the intensity of the CW-IRSL signal, with the only difference being that the amount of shifting along the time-axis is now given by Equation (21) instead of Equation (9).

The experimental data in the next two sections will be used to test the following predictions from these analytical equations:

(a) The luminescence intensities for the thermally/optically treated and the untreated samples can be fitted with the same equation.
(b) When the luminescence decay curve $L(t)$ for the thermally/optically treated sample is shifted along the time-axis by a quantity T, the two luminescence decay curves (either CW-IRSL or CW-OSL, depending on the experiment) can be expected to fall on top of each other.
(c) The amount of shifting T of the time-axis is predicted to depend linearly on the preheat time t_{PH} or on the optical bleaching time t_{BLEACH}, depending on the type of experiment being carried out.

An additional prediction which is not tested in this paper is that the amount of shifting T of the time-axis will depend also on the preheat temperature T_{PH} via the Boltzmann factor $e^{-E_{thermal}/kT_{PH}}$. This prediction was tested recently by Jain et al. (2015) and is discussed in the Discussion section of this paper.

3. Experimental

The luminescence signals from the feldspar samples used in this paper have been studied previously in Polymeris et al. (2013). These authors investigated the possibility of using thermoluminescence (TL) for structural characterization of ten K-feldspar samples. They found a good correlation between TL sensitivity and individual K-feldspar structure and suggested that these samples are ideal for investigating basic TL, OSL and IRSL signals. The group of samples studied by these authors consisted of 3 sanidine, 4 orthoclase and 3 microcline feldspars.

The experimental setup, sample preparation and experimental conditions for the present paper were described previously in Polymeris et al. (2013, 2014). TL measurements were carried out using a Riso TL/OSL reader (model TL/OSL-DA-15), equipped with a $^{90}Sr/^{90}Y$ beta particle source, delivering a nominal dose rate of 0.075 Gy/s. A 9635QA photomultiplier tube was used with a 7.5 mm Hoya U-340 filter (~340 nm, FWHM ~80 nm). All necessary heating was performed in a nitrogen atmosphere with a low constant heating rate of 2 °C/s, in order to avoid significant temperature lag. The OSL stimulation wavelength is 470 (±20) nm for the case of blue stimulation, delivering at the sample position a maximum power of 40 mW/cm^2. For IRSL, the stimulation wavelength is 875 (±40) nm and the maximum power ~135 mW/cm^2.

Two of the samples studied previously in Polymeris et al. (2013) are used in this paper, namely microcline sample KST4 and orthoclase sample VRS3 (see Polymeris et al., 2013; their Table 1).

Two different experimental protocols were used in order to test the equations in the previous sections, as follows.

3.1. Protocol #1

This is a double procedure as described in Section 2.1. An irradiated aliquot of feldspar sample KST4 is first exposed to a fixed preheat temperature of 300 °C for a variable preheating time t_{PH}, followed by measurement of its CW-IRSL signal. The specific steps in the protocol are:

Step 1 Test dose 40 Gy
Step 2 Preheat at temperature T_{PH} = 300 °C for preheat time t_{PH} = 0, 1, 3, 5, 10, 17, 25, 37, 50, 75 s. The case of t_{PH} = 0 corresponds to the unheated sample.
Step 3 Measurement of CW-IRSL signal for 2000 s at 50 °C.
Step 4 Repeat steps 1–3 for a new preheat time t_{PH}.

3.2. Protocol #2

This is a double procedure similar to the one described in Section 2.2. An aliquot of sample KST4 is first exposed to infrared light (CW-IRSL) for a variable bleaching time T_{BLEACH}, followed by measurement of its CW-OSL signal. The specific steps in the protocol are:

Step 1 Test dose 40 Gy.
Step 2 Optical bleaching using CW-IRSL at room temperature for time $T_{BLEACH} = T_{BLEACH}$ = 0, 5, 10, 25, 35, 50, 75, 100, 250, 500 and 1000 s. The case of T_{BLEACH} = 0 corresponds to the unbleached sample.
Step 3 Measurement of CW-OSL signal at room temperature for 1000 s
Step 4 TL measurement up to a temperature T = 500 °C at 20 °C/s.
Step 5 Repeat steps 1–4 for a new CW-IRSL stimulation time T_{BLEACH}.

Both experimental protocols described above were applied using a single aliquot, and this makes necessary testing for sensitivity changes which may occur during the experiments. The sensitivity test for protocol #1 was performed by measuring the CW-IRSL signals before and after the end of the protocol. The sensitivity test for protocol #2 was performed by applying an additional TL readout up to 500 °C between steps 4 and 5, after the stimulation times 10,50, 250 and 1000 s. It was found that the sensitivities of all samples showed an excellent stability and that the reproducibility of the signals was better that 2%. It was concluded that there was no need for applying sensitivity corrections.

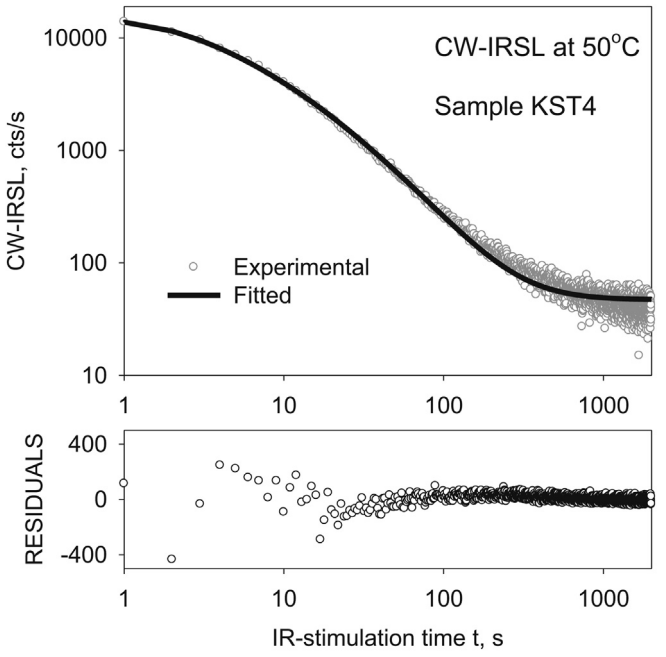

Fig. 1. Typical example of fitting the CW-IRSL curves from protocol #1 with Equation (17), for a freshly irradiated aliquot of feldspar sample KST4, measured at 50 °C. The CW-IRSL curve is fitted using Equation (17), with residuals of the fitting procedure shown underneath the graph.

4. Experimental results

4.1. Results from protocol #1

Fig. 1 shows a typical CW-IRSL decay curve from a freshly irradiated sample KST4, measured at 50 °C during protocol #1. The sample was preheated for 3 s at 300 °C and it is assumed that there is no time-shift necessary for this set of data (T = 0 in Equation (9)).

Fig. 2 shows a typical example of shifting a CW-IRSL curve measured with a preheating time t_{PH} = 37 *s* along the horizontal time-axis, resulting in the shifted CW-IRSL curve falling on top of the CW-IRSL curve for the reference curve (t_{PH} = 3 *s*). Fig. 3(a) shows the result of shifting all the CW-IRSL curves measured at different preheating times along the time-axis, resulting in all

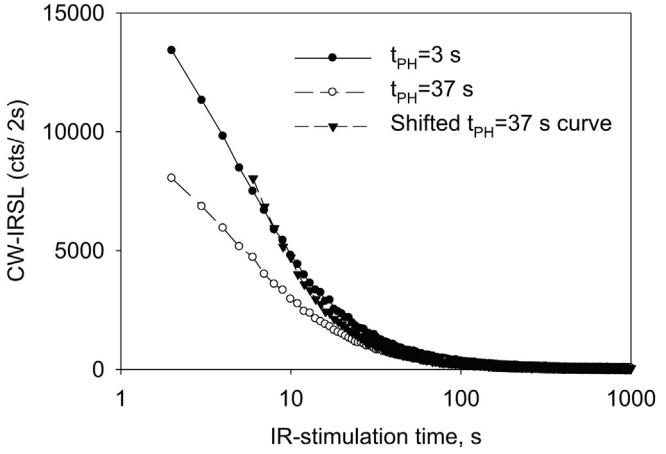

Fig. 2. A typical example of shifting a CW-IRSL curve measured with a preheating time t_{PH} = 37 *s* along the horizontal time-axis, resulting in the shifted CW-IRSL curve falling on top of the CW-IRSL curve for the reference curve (t_{PH} = 3 *s*).

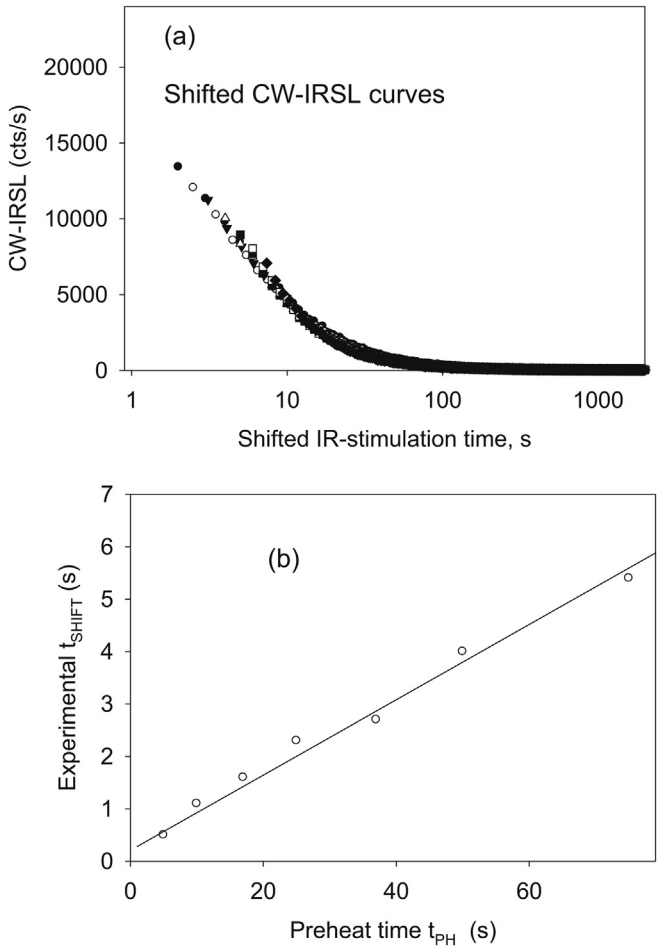

Fig. 3. (a) Shifting all the CW-IRSL curves measured at different preheating times along the time-axis results in all curves overlapping, within the accuracy of the experimental data. The CW-IRSL curve for $t_{PH} = 3$ *s* is used as a reference curve. (b) The experimentally determined time-shifts (t_{SHIFT}) from (a), as a function of the preheating times t_{PH}. The linear dependence is in agreement with the derived Equation (9).

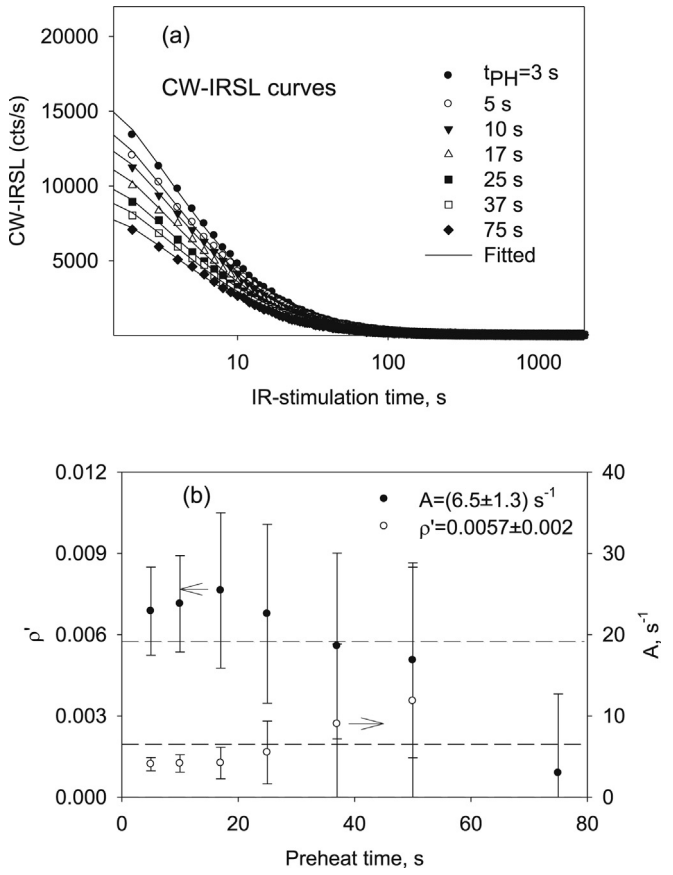

Fig. 4. (a) The results of fitting all experimental CW-IRSL curves obtained in protocol #1 for different preheat times using Equation (17) and with the values of the time shifting obtained from Fig. 3b. The fitted curves are shown by the solid lines. (b) The fitting parameters obtained at different preheating times by analyzing the time-shifted experimental data. The error bars are estimated from the best fitting procedure.

curves overlapping, at least within the experimental accuracy of the data. The first three measured CW-IRSL curves for preheat times $t_{PH} = 0,1,3$ *s* were essentially identical, so we used the CW-IRSL curve for $t_{PH} = 3$ *s* for our reference curve for the untreated sample. Fig. 3(b) shows the experimentally determined time-shifts (t_{SHIFT}) from Fig. 3(a) (by using the technique shown in Fig. 2), as a function of the preheating times t_{PH}. The linear dependence shown in Fig. 3(b) is in agreement with the derived Equation (9).

Fig. 4 shows the results of fitting all experimental CW-IRSL curves obtained in protocol #1 for different preheat times t_{PH} using Equation (17) and with the values of the time shifting obtained from Fig. 3(b). The fitted curves are shown by the solid lines in Fig. 4(a) indicating excellent fits to the experimental data. Fig. 4(b) shows the fitting parameters ρ', A obtained at different preheating times by analyzing the time-shifted experimental data. The values of the fitting parameters are seen to be practically constant at all preheating times, with the average dimensionless charge density given by $\rho' = 0.006 \pm 0.002$ and the average IR stimulation probability by $A_{IR} = 6.5 \pm 1.3\ s^{-1}$. The error bars in Fig. 4(b) are estimates obtained from the best fitting procedure.

4.2. Results from protocol #2

Fig. 5(a) shows a typical CW-OSL decay curve from a freshly irradiated sample KST4, measured during protocol #2. The CW-OSL curve is also fitted using Equation (17) and it was found that this equation provides excellent fits to all experimental CW-OSL curves obtained in protocol #2 for different IR bleaching times t_{BLEACH}, as shown by the fitted curves in Fig. 7(a). Fig. 5(b) shows the fitting parameters ρ', A obtained at different IR bleaching times, with the average dimensionless charge density given by $\rho' = 0.0046 \pm 0.0004$ and the average blue light stimulation probability by $A = 3.9 \pm 0.8\ s^{-1}$.

Fig. 6 shows a typical example of shifting a CW-OSL curve measured with a bleaching time $t_{BLEACH} = 100\ s$ along the horizontal time-axis, resulting in the shifted CW-OSL curve falling on top of the curve for the unheated sample ($t_{BLEACH} = 0\ s$). Fig. 7 shows the result of shifting along the time-axis all the CW-OSL curves measured at different bleaching times t_{BLEACH}, resulting in all curves overlapping, at least within the experimental accuracy of the data.

Fig. 8 shows the experimentally determined time-shifts (t_{SHIFT}) from Fig. 7(b), as a function of the IR bleaching times t_{BLEACH}. The experimental data shows that the dependence is linear at least for bleaching times $t_{BLEACH} \leq 100\ s$, with a non-linear dependence shown in the inset of Fig. 8 for higher times t_{BLEACH}. The linearity shown in Fig. 8 is in agreement with the derived Equation (21), at least for $t_{BLEACH} \leq 100\ s$.

As discussed in Section 2.2, the main assumption in deriving the equations is that the blue light (CW-OSL) accesses the same charge density ρ' as the IR light (IRSL), but with a different optical stimulation probability. This assumption is tested by fitting the CW-IRSL

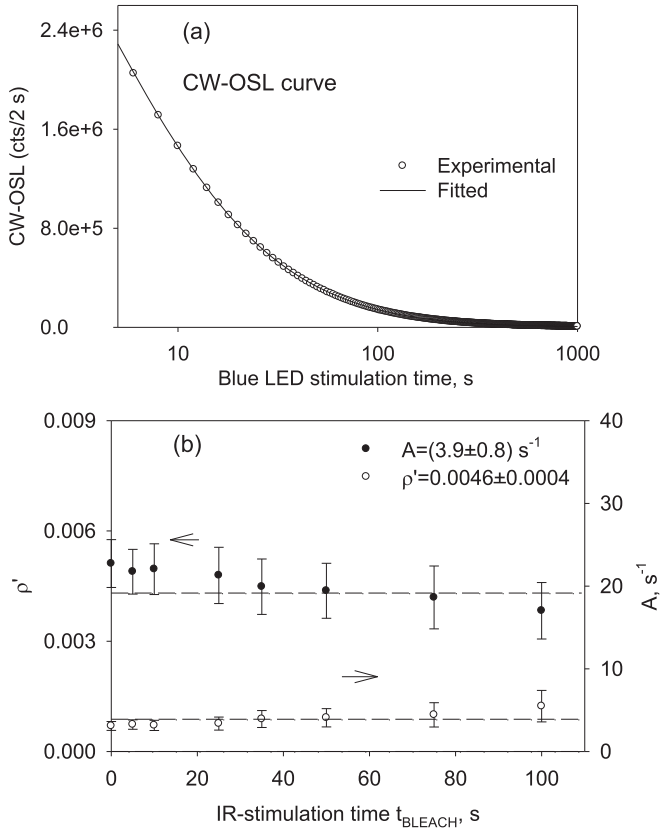

Fig. 5. (a) A typical CW-OSL decay curve from a freshly irradiated sample KST4, measured during protocol #2. The CW-OSL curve is fitted using Equation (17). (b) The parameters ρ', A extracted from fitting the experimental data in protocol #2, as a function of the IR bleaching time t_{BLEACH}.

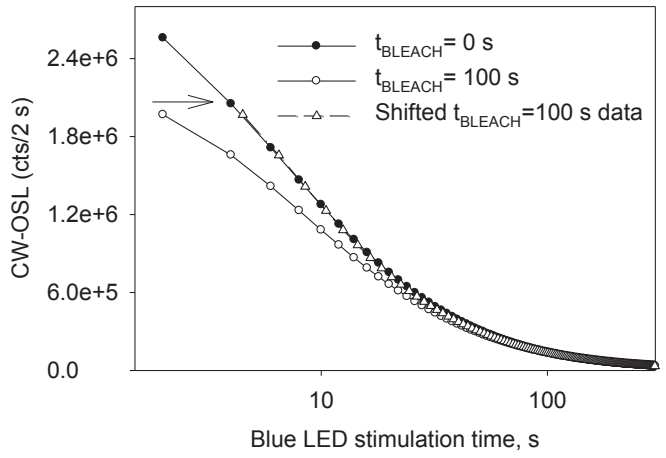

Fig. 6. A typical example of shifting a CW-OSL curve measured with a bleaching time $t_{BLEACH} = 100\ s$ along the horizontal time-axis, resulting in the shifted CW-OSL curve falling on top of the curve for the unheated sample ($t_{BLEACH} = 0\ s$).

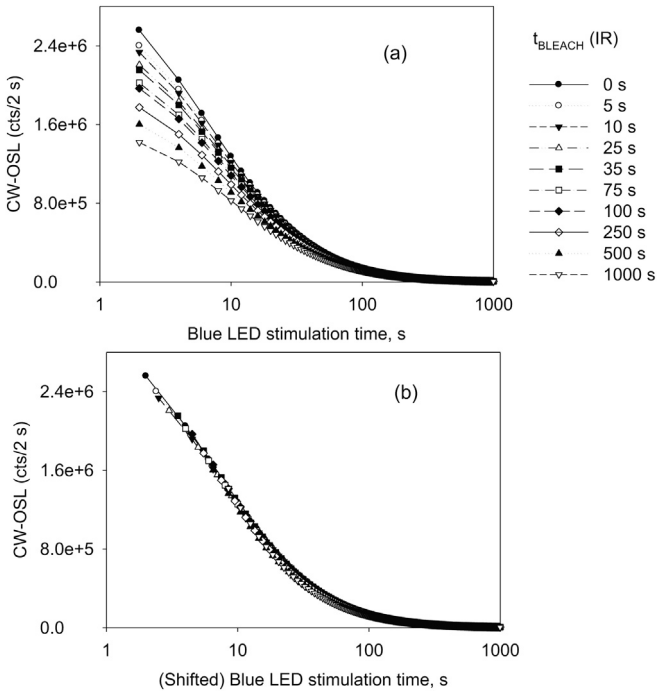

Fig. 7. (a)–(b) Shifting of all the CW-OSL curves measured at different bleaching times along the time-axis, results in all curves overlapping, at least within the experimental accuracy of the data. The CW-OSL curves in (a) are fitted using Equation (17), shown by the fitted curves in (a).

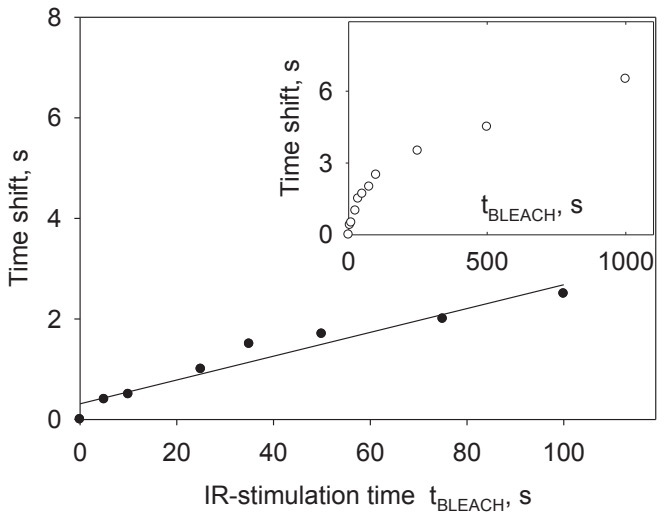

Fig. 8. The experimentally determined time-shifts (t_{SHIFT}) from Fig. 7 are shown as a function of the IR bleaching times t_{BLEACH}. The dependence is linear at least for bleaching times $t_{BLEACH} \leq 100\ s$, with a non-linear dependence shown in the inset for higher times t_{BLEACH}. The linearity shown here is in agreement with the derived Equation (26).

curve measured in step 3 of protocol #2, using Equation (17). The fitting process of the CW-IRSL curve in Fig. 9 yields a charge density value of $\rho' = 0.0056 \pm 0.0001$, which is in reasonably close agreement with the value of $\rho' = 0.0046 \pm 0.0004$ obtained from the analysis of the CW-OSL curves in Fig. 5(b). It is concluded that the CW-OSL and CW-IRSL signals most likely stem from the same trap, characterized by the same value of ρ'.

Fig. 10(a) shows the result of repeating the measurements in protocol #2 for a second sample, an orthoclase sample VRS3 previously studied by Polymeris et al. (2013). The results are shown in Fig. 10(b), with the time-shifted CW-OSL curves falling on top of each other. This second apatite sample also showed a linear dependence of the time shifts on the IR bleaching time at least for bleaching times $t_{BLEACH} \leq 100\ s$, similar to microcline sample KST4.

The experimental data in this section provided a rather surprising result, by the application of the localized transition model to blue light stimulation. Since blue light can be expected to raise

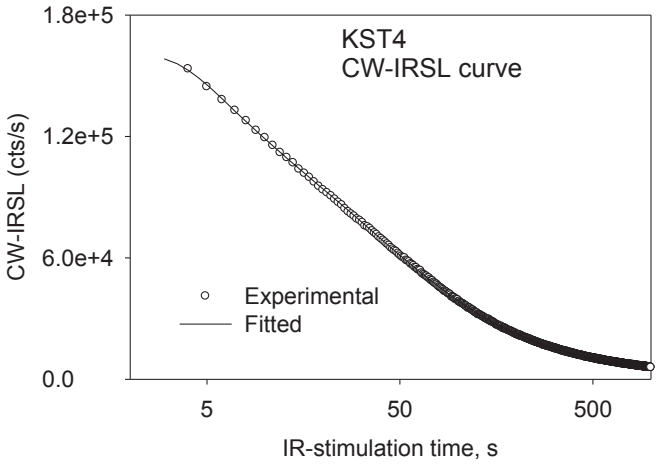

Fig. 9. Fitting of the CW-IRSL curve measured in step 3 of protocol #2, using Equation (17).

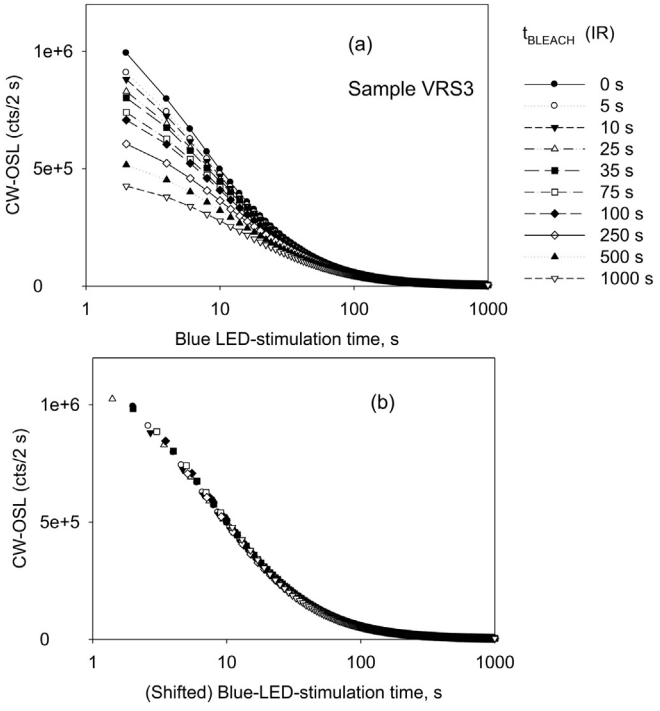

Fig. 10. The experiment in Fig. 7 was repeated for a second feldspar sample VRS3, with similar results.

electrons into the conduction band, then the results of the experiment should not strictly follow localized recombination. It is not clear whether this experimental result will hold for different types of samples and for different optical bleaching conditions. Perhaps the best method of ascertaining the validity of these results is by studying this effect using stimulating light from LEDs with different wavelengths, ranging from blue to green.

5. Discussion and conclusions

Recently (Jain et al., 2015) extended their localized transition model to include Arrhenius analysis and truncated nearest neighbor distributions. Their extended model provided a better understanding of charge depletion and of the shape of the luminescence decay curves. An important difference between the extended model of Jain et al. (2015) and the work in this paper is that they consider the truncated distributions of nearest neighbors, while our derivation is based on the analytical equations derived by Pagonis et al. (2013) and on the series approximation by Tachiya and Mozumder (1974).

The model of Jain et al. (2015) and the equations they derive are more general than the luminescence intensity equations in this paper. Specifically our results in Equation (17) are a special case of the more general equation by Jain et al. (2015), with the substitutions $b = s$ and $\tau = zT$, where T is an arbitrary parameter with units of time. In the present paper we derived new analytical equations for the time shifting of the CW-IRSL signals (Equations (9) and (21)).

Jain et al. (2015) arrived at the conclusion that shifting the time-axis in a double preheating/CW-IRSL experiment can cause the CW-IRSL curves to lie on top of each other. This conclusion was also reached in the work in this paper.

The experimental data in Jain et al. (2015) describe a situation in which the preheat time is constant (10 s) and they varied the preheat temperature T_{PH}, while in our experiment the preheat temperature was fixed at $T_{PH} = 300$ °C and the preheat time was varied in the interval $t_{PH} = 0–75$ s.

There are several conditions which must be met when using the analytical equations in this paper:

(a) The CW-IRSL or CW-OSL signals must contain a single tunneling component, as determined by fitting the experimental data with Equation (17). Many luminescence signals from feldspars and apatites contain such a single tunneling component, while other samples studied by us were found to contain at least two tunneling components (Sfampa et al., 2015, 2014; Polymeris et al., 2014).

(b) The equations should apply to any double procedure such as those discussed in Section 2, as long as the stimulation probabilities involved in the two stages are constant (e.g. isothermal heating, optical stimulation with blue light LEDs, infared stimulation).

Clearly more experimental work is required to decide whether IRSL and OSL are indeed always accessing the same charge density, and whether the results apply to feldspars as well as to apatite samples.

Acknowledgments

The authors would like to thank Dr. Eleni Theodosoglou for providing the pure K-feldspar samples.

References

Bailiff, I.K., Poolton, N.R.J., 1991. Studies of charge transfer mechanisms in feldspars. Nucl. Tracks Radiat. Meas 18, 111–118.
Bøtter-Jensen, L., McKeever, S.W.S., Wintle, A.G., 2003. Optically Stimulated Luminescence Dosimetry. Elsevier Science B.V., Amsterdam, p. 355.
Bulur, E., 1996. An alternative technique for optically stimulated luminescence (OSL) experiment. Radiat. Meas. 26, 701–709.
Chruścińska, A., 2001. The fractional glow technique as a tool of investi-gation of TL bleaching efficiency in K-feldspar. Geochronometria 20, 21–30.
Duller, G.A.T., 1994. A new method for the analysis of infrared stimulated luminescence from potassium feldspars. Radiat. Meas. 23, 281–285.
Duller, G.A.T., 1995. Infrared bleaching of the thermoluminescence of four feldspars. J. Phys. D. Appl. Phys. 28 (6), 1244–1258. http://dx.doi.org/10.1088/0022-3727/28/6/030.
Duller, G.A.T., Bøtter-Jensen, L., 1993. Luminescence from potassium feldspars stimulated by infrared and green light. Radiat. Prot. Dosim. 47, 683–688.
Duller, G.A.T., Wintle, A.G., 1991. On infrared stimulated luminescence at elevated temperatures. Nucl. Tracks Radiat. Meas. 18, 379–384.
Huntley, D.J., 2006. An explanation of the power-law decay of luminescence. J. Phys.

Cond. Matt 18, 1359–1365.
Jain, M., Ankjærgaard, C., 2011. Towards a non-fading signal in feldspar: Insight into charge transport and tunnelling from time-resolved optically stimulated luminescence. Radiat. Meas. 46, 292–309.
Jain, M., Guralnik, B., Andersen, M.T., 2012. Stimulated luminescence emission from localized recombination in randomly distributed defects. J. Phys. Condens. matter 24, 385402.
Jain, M., Sohbati, R., Guralnik, B., Murray, A.S., Kook, M., Lapp, T., Prasad, A.K., Thomsen, K.J., Buylaert, J.P., 2015. Kinetics of infrared stimulated luminescence from feldspars. Radiat. Meas. (in press) http://dx.doi.org/10.1016/j.radmeas.2015.02.006.
Kitis, G., Pagonis, V., 2013. Analytical solutions for stimulated luminescence emission from tunnelling recombination in random distributions of defects. J. Lumin. 137, 109–115.
Kitis, G., Pagonis, V., 2014. Properties of thermoluminescence glow curves from tunneling recombination processes in random distributions of defects. J. Lumin. 153, 118–124.
Li, B., Li, S.-H., 2013. The effect of band-tail states on the thermal stability of the infrared stimulated luminescence from K-feldspar. J. Lumin. 136, 5–10. http://dx.doi.org/10.1016/j.jlumin.2012.08.043.
Morthekai, P., Thomas, J., Padian, M.S., Balaram, V., Singhvi, A.K., 2012. Variable range hopping mechanism in band-tail states of feldspars: a time-resolved IRSL study. Radiat. Meas. 47, 857–863.
Murray, A.S., Buylaert, J.P., Thomsen, K.J., Jain, M., 2009. The effect of preheating on the IRSL signal from feldspar. Radiat. Meas. 44, 554–559.
Pagonis, V., Phan, H., Ruth, D., Kitis, G., 2013. Further investigations of tunneling recombination processes in random distributions of defects. Radiat. Meas. 58, 66–74.
Pagonis, V., Jain, M., Thomsen, K.J., Murray, A.S., 2014a. On the shape of continuous wave infrared stimulated luminescence signals from feldspars: a case study. J. Lumin. 153, 96–103.
Pagonis, V., Morthekai, P., Kitis, G., 2014b. Kinetic analysis of thermoluminescence glow curves in feldspars: evidence for a continuous distribution of energies. Geochronometria 41, 168–177.
Polymeris, G.S., Theodosoglou, E., Kitis, G., Tsirliganis, N.C., Koroneos, A., Paraskevopoulos, K.M., 2013. Preliminary results on structural state characterization of K-feldspars by using thermoluminescence. Mediterr. Archaeol. Archaeom. 13, 155–161.
Polymeris, G.S., Giannoulatou, V., Sfampa, I., Tsirliganis, N.C., Kitis, G., 2014. Search for stable energy levels in materials exhibiting strong anomalous fading; the case study of apatites. J. Lumin. 153, 245–251.
Sfampa, I.K., Polymeris, G.S., Tsirliganis, N.C., Pagonis, V., Kitis, G., 2014. Prompt isothermal decay of thermoluminescence in an apatite exhibiting strong anomalous fading. Nucl. Instrum. Meth. B 320, 57–63.
Sfampa, I.K., Polymeris, G.S., Pagonis, V., Thodosoglou, E., Tsirliganis, N.C., Kitis, G., 2015. Correlation of basic TL, OSL and IRSL properties of ten K-feldspar samples of various origin. Nucl. Instrum. Meth. B 359, 89–98.
Tachiya, M., Mozumder, A., 1974. Decay of trapped electrons by tunnelling to scavenger molecules in low temperature glasses. Chem. Phys. Lett. 28, 87–89.
Thomsen, K.J., Murray, A.S., Jain, M., 2011. Stability of IRSL signals from sedimentary feldspars. Geochronometria 38 (1), 1–13.
Visocekas, R., Spooner, N.A., Zink, A., Blank, P., 1994. Tunnel afterglow, fading and infrared emission in thermoluminescence of feldspars. Radiat. Meas. 23, 377–385.